Science of the Total Environment 598 (2017) 1140–1150

Contents lists available at ScienceDirect

Science of the Total Environment

journal homepage: www.elsevier.com/locate/scitotenv

Zero-valent iron-facilitated reduction of nitrate: Chemical kinetics and reaction pathways

Yiping Zhang [a], Grant B. Douglas [b], Long Pu [c], Quanlin Zhao [a], Yan Tang [c], Wei Xu [c], Bihuan Luo [c], Wei Hong [c], Lili Cui [d], Zhengfang Ye [a,*]

[a] Department of Environmental Engineering, Peking University, The Key Laboratory of Water and Sediment Sciences, Ministry of Education, Beijing 100871, China
[b] CSIRO Land and Water, Centre for Environment and Life Sciences, Private Bag 5, Wembley, 6913, WA, Australia
[c] Sichuan Jinsha Nano Technology Co., Ltd., Panzhihua Vanadium and Titanium Industrial Park, Panzhihua, Sichuan Province 730900, China
[d] Zhangjiakou, Hebei Energy and Environmental Engineering, Hebei Institute of Architectural Engineering, Hebei 075000, China

HIGHLIGHTS

- This study has focused on a simple, low pH denitrification methodology with a view to ready industrial-scale application.
- The kinetics and mechanisms of the reduction of NO_3^- in solution to NH_3 by $ZVI_{1.5}$ particles has been examined.
- Denitrification by $ZVI_{1.5}$ is primarily a pH-dependent, surface-mediated process.
- The generation of Fe^{2+} and NO_2^- intermediates prior to formation of Fe^{3+} oxyhydroxide (goethite) and NH_3.

GRAPHICAL ABSTRACT

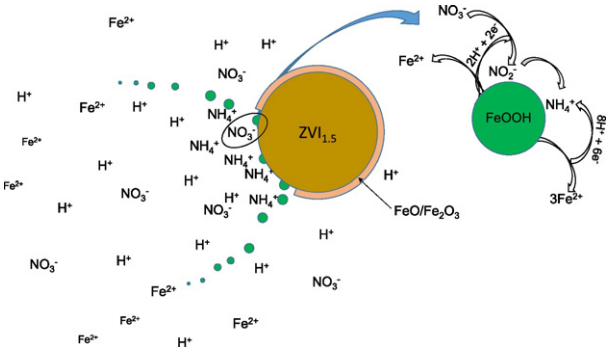

ARTICLE INFO

Article history:
Received 20 February 2017
Received in revised form 7 April 2017
Accepted 9 April 2017
Available online 5 May 2017

Editor: J Jay Gan

Keywords:
Zero-valent iron (ZVI)
Denitrification
Kinetics
Reaction pathway

ABSTRACT

The kinetics and mechanisms of the reduction of NO_3^- in solution to NH_3 by 1.5 μm diameter zero-valent iron ($ZVI_{1.5}$) particles has been examined. The effects of initial pH, $ZVI_{1.5}$ particle concentration and initial NO_3^- concentration were also investigated. Results indicate that denitrification by $ZVI_{1.5}$ is primarily a pH-dependent, surface-mediated process. At an initial $ZVI_{1.5}$ concentrations of 0.832 g/L, and an optimal initial pH of 1.62, the NO_3^- concentration was reduced by 95% from 12.50 mg/L-N to 0.65 mg/L-N, in 120 min. Several kinetic models were used to describe the denitrification process based on the $ZVI_{1.5}$:NO_3^- ratio. Based on mineralogical and surface analysis of the reacted $ZVI_{1.5}$, and detailed solution chemical analysis, the denitrification reaction pathway involves oxidation and partial dissolution of the $ZVI_{1.5}$ with the generation of Fe^{2+} and NO_2^- intermediates prior to formation of Fe^{3+} oxyhydroxide (goethite) and NH_3.

1. Introduction

Zero-valent iron (ZVI) has been extensively investigated for treatment of environmental contaminants in the biosphere (Fewtrell, 2004; Kapoor and Viraraghavan, 1997). Examples of the application of

* Corresponding author.
E-mail address: zhengfangye@163.com (Z. Ye).

http://dx.doi.org/10.1016/j.scitotenv.2017.04.071
0048-9697/

ZVI include the degradation of chlorinated organic compounds (Audi-Miro et al., 2015; Waclawek et al., 2015; Zhang et al., 2015; Belghit et al., 2015; Zhou et al., 2014a, 2014b), polychlorinated biphenyls (PCBs, (Olson et al., 2014; Long et al., 2014; Jun et al., 2013)), removal of heavy metals (Han et al., 2016; Simeonidis et al., 2016; Guo et al., 2016; Li et al., 2015a, 2015b), and a range of inorganic compounds (Simeonidis et al., 2016; Sismanoglu et al., 2015; Soleymanzadeh et al., 2015; Liu et al., 2013) from both wastewaters and groundwater. The utility of ZVI in contaminant degradation or absorption is principally related to its high specific surface area and surface reactivity (Zhou et al., 2014a, 2014b; Schwindaman et al., 2014).

In Fe^0-H_2O system, zero-valent iron (ZVI) functions as an electron donor, while corresponding pollutants function as electron acceptor.

$$Fe^0 \rightarrow Fe^{2+} + 2e^- \quad (1)$$

Both water and dissolved oxygen may also be involved in ZVI-mediated transformation according to the following reactions.

$$2H_2O + 2e^- \rightarrow 2OH^- + H_2 \quad (2)$$

$$2H_2O + O_2 + 4e^- \rightarrow 4OH^- \quad (3)$$

Therefore, three possible reaction mechanisms may occur in Fe^0-H_2O system with one or more of Fe^0, Fe^{2+}, H_2 playing an important role: (Luo et al., 2014; Ling et al., 2015) via

(1) electron transfer from Fe^0 directly on the surface of the ZVI,
(2) electron transfer indirectly via Fe^{2+}, or
(3) electron transfer by H_2 with the ZVI (Fe^0) surface acting as a catalytic surface to promote the production of H_2.

With the development of industry and intensive agriculture, considerable quantities of nitrogen compounds have accumulated in the environment including from the application of nitrogenous fertilizers, the discharge of industrial wastewaters, animal manure, septic waste, and atmospheric deposition from nitrogen oxide emission (Jung et al., 2011). Consequently, nitrogen compounds may contaminate both surface and groundwater in the form of NO_3^-, in some cases resulting in the contamination of drinking water sources (Fagan et al., 2016; Zhang et al., 2016). Nitrate may be reduced to nitrite in blood and result in methemoglobinemia or "blue-baby" syndrome in susceptible children (Kapoor and Viraraghavan, 1997; Kay et al., 2004).

Conventionally, NO_3^- in water can be removed by various technologies. These may include biological denitrification, ion exchange, reverse osmosis, and chemical reduction. (Schwindaman et al., 2014; Zhou et al., 2014a, 2014b; Ren et al., 2015; An et al., 2014; Su et al., 2014a, 2014b). Considerable research related to chemical reduction of NO_3^- by zero-valent iron (ZVI) has been undertaken since the 1990s (Yang and Lee, 2005), as this method often enables high denitrification rates (Ren et al., 2015). While denitrification via nanoscale ZVI could occur under a wide range of pH (i.e., 3–11), the pH of the water also increases in the presence of nZVI because of the significant anaerobic corrosion of Fe^0 (Lin et al., 2008), millimeter-scale ZVI could only denitrify under acidic conditions (pH < 4) (Yoshino and Kawase, 2013). However, it has been reported that the addition of HEPES (4-(2-hydroxyethyl)-1-piperazineethanesulfonic acid) buffer could expand the reaction pH of ZVI to neutral pH (Luo et al., 2014).

When applied to denitrification, different types of ZVI may exhibit a range of reaction kinetics under different reaction conditions. Many denitrification experiments may be explained using a pseudo-first order kinetic equation (Penon et al., 2016; Cho et al., 2015; Peng et al., 2015; Siciliano, 2015; Jiang et al., 2015; Zhou et al., 2015; Ling et al., 2015). Alternatively, a reaction order of 1.7 was found using 6–10 μm ZVI and a ratio of 384 g ZVI to 1 mol NO_3^- (Huang et al., 1998). The observed kinetics (k_{obs}) value was determined to be 0.035 $L^{0.7}/mg^{0.7}\cdot min^1$ when the initial NO_3^- concentration was 50 mg/L in the presence of 0.05 mol sulfate. (Yang and Lee, 2005) studied several aspects of chemical reduction of nitrate by synthesized nanoscale iron particles, showing that a first- or pseudo-first-order kinetic model may not be suitable to describe the kinetics of the reaction. Ammonia is the principal denitrification reaction product in the presence of ZVI in addition to N_2 gas (Zhao et al., 2015; Huang et al., 2015; Cho et al., 2015; Guo et al., 2015; Peng et al., 2015; Ma et al., 2015; Jiang et al., 2015). According to (Devlin et al., 2000), the Gibbs free energy of the two main reactions indicate that it is more thermodynamically favorable to produce NH_3 than N_2:

$$4Fe^0_{(s)} + NO^-_{3(aq)} + 9H^+_{(aq)} \rightarrow 4Fe^{2+}_{(aq)} + NH_{3(aq)} + 3H_2O(l) \quad -942KJ/mol \quad (4)$$

$$5Fe^0_{(s)} + 2NO^-_{3(aq)} + 12H^+_{(aq)} \rightarrow 5Fe^{2+}_{(aq)} + N_{2(aq)} + 6H_2O(l) \quad -797KJ/mol \quad (5)$$

while as a consequence of hydrogen ion consumption, the solute pH rises during the reaction (Shin and Cha, 2008; Choe et al., 2004).

While it is generally recognized that NO_3^- adsorption and a subsequent redox reaction is the principal mechanism of ZVI denitrification (Wang et al., 2014; Liu et al., 2014; Su et al., 2014a, 2014b), previous studies have documented that a range of factors may influence the mass transfer rate of surface reaction and hence, the efficiency of denitrification. These factors may include mixing intensity (Choe et al., 2004), initial acidity (Zhang et al., 2011; Hwang et al., 2011), ZVI dose (Fateminia and Falamaki, 2013; Hosseini et al., 2012), and the initial NO_3^- concentration (Zawaideh and Zhang, 1998).

Based on the studies reviewed above, the aim of this study was to elucidate the chemical reduction of NO_3^- by 1.5 μm diameter ZVI, hereafter referred to as $ZVI_{1.5}$, and in particular, the transformation of the $ZVI_{1.5}$ and the surface reactions involved in a strongly acidic media. In addition, the effects of varying pH, temperature, oxygen, $ZVI_{1.5}$ dose, and the initial NO_3^- concentration on denitrification were also investigated. A simple kinetic model was also developed to describe the denitrification process. Both X-ray diffraction (XRD) and X-ray photoelectron spectroscopy (XPS) were used to determine the surface reaction products of the $ZVI_{1.5}$ produced during denitrification.

Significantly, direct denitrification of NO_3^- to NH_4^+ in acidic solutions without prior pH neutralization as undertaken in this study offers an alternative treatment pathway, particularly in effluents produced from major industrial processes such as nitric acid-based mineral dissolution (Cheng et al., 2014). Hence, this study has focused on a simple, low pH denitrification methodology with a view to ready industrial-scale application.

The ZVI particle size is also known to have significant effects on reactivity and reaction kinetics (Dong et al., 2010). In this study, $ZVI_{1.5}$ was chosen due to its and ZVI materials with similar particle size distributions widespread commercial availability.

2. Materials and methods

2.1. Materials

The ZVI used in the experiments, as provided by Sichuan Jinshanami Technology Co. Ltd., China, was approximately 1.5 μm in it smallest axis, with a bulk density of 0.95 g/c, and with Brunauer–Emmett–Teller (BET) surface area of 1.27 m^2/g. Other chemicals (KNO_3, HCl) were purchased from the Beijing Chemical Plant, China and were of at least analytical grade.

2.2. Methods

Denitrification batch experiments were conducted in 1.5 L Erlenmeyer flasks (Fig. 1). Each flask was filled with 1200 mL of reactant

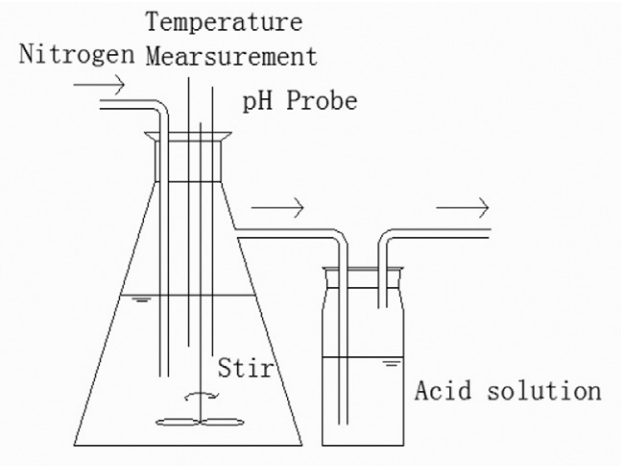

Fig. 1. Schematics of the $ZVI_{1.5}$ denitrification batch reactor.

solution made by containing 25 mg/L NO_3^--N as KNO_3 in distilled water and the solution was purged with nitrogen gas before the addition of the $ZVI_{1.5}$. Anoxic conditions were maintained by continuous purging of nitrogen gas (1 L/min) through the reactor. Different masses of $ZVI_{1.5}$ (0.104, 0.416, 0.832 g/L) were added to the reactor according to the experiment undertaken. Solution samples were taken at 0, 2, 5, 10, 15, 30, 60, and 120 min and filtered through 0.22 μm syringe filters prior to analysis. The $ZVI_{1.5}$ suspension was continuously stirred by an electric stirrer with the reaction temperature maintained at 20 °C. The off-gas from the reactor was bubbled through 200 mL of an acidic solution throughout the entire reaction for the analysis of produced NH_3.

The concentration of NO_3^-, NO^-_2, NH^+_4, and Fe^{2+} were determined colorimetrically by UV spectrophotometer (UV1800, Shimadzu) according to Chinese Environment standards HJ/T 346-2007, GB 7493-87, HJ/T 535-2009, and HJ/T 345-2007. Control denitrification experiments containing no $ZVI_{1.5}$ particles were also prepared. pH was measured using a HANNA pH-201 m. The BET surface area was measured by N_2 adsorption isotherms at 77 K using an automated surface area and pore size analyzer (ASAP 2010, Micromeritics, USA).

The surface morphologies of $ZVI_{1.5}$ before and after reaction was observed using a Quanta 200FEG environmental scanning electron microscope (SEM, FEI Company, USA), with the accelerating voltage of 15 kV.

X-ray diffraction analysis (XRD), X'Pert Pro, PANalytical, was performed on ZVI samples to detect post-reaction mineralogical changes in the ZVI. The scan ranged from 10 to 90° 2θ with a scan speed of 1° min^{-1}, an operating voltage of 40 kV, a current of 100 mA, and k = 01541 nm.

X-ray photoelectron spectroscopy (XPS) was used to determine changes in the chemical binding of iron species on the surface of $ZVI_{1.5}$ and the surface chemical composition. The spent $ZVI_{1.5}$ sample was carefully packed on a XPS sampling template under anaerobic conditions to avoid surface oxidation. The XPS analysis was undertaken using an Axis Ultra (Kratos Analytical Ltd., JP) with an Al kα X-ray (1486.7 eV) with a 200 W power source. Raw spectra were smoothed before being fitted using a Shirley base line and a Gaussian–Lorentzian shape peak. Narrow scanned spectra were used to obtain the chemical state of the Fe.

2.3. Kinetic model

Nitrate reduction kinetics have generally been described by a (pseudo) first order reaction, however, this model order is not relevant under ZVI- or nZVI-limiting conditions (Alidokht et al., 2011). Nitrate removal and ammonia generation have been successfully described as adsorption and heterogeneous catalytic reaction, respectively (Kim et al., 2016). Several kinetic models, including the pseudo-first-order reaction model, pseudo-first-order adsorption, the pseudo-second-order adsorption, the double constant equation (Xu et al., 2017; Deliyanni et al., 2007), and the intra-particle diffusion model were evaluated in this study. The way they describe the behavior of nitrate is expressed as follows:

$$\frac{dC_n}{dt} = -k_{k1}C_n \tag{6}$$

$$\frac{dC_n}{dt} = -k_m C_n^n \tag{7}$$

$$\frac{dq_n}{dt} = -k_{a1}(q_{n,e} - q_n), -\frac{dC_n}{dt} = -k_{a1}(C_n - C_{n,e}) \tag{8}$$

$$\frac{dq_n}{dt} = -k_{a1}(q_{n,e} - q_n)^2, -\frac{dC_n}{dt} = -k_{a1}(C_n - C_{n,e})^2 \tag{9}$$

$$R = k_{id} \cdot t^{\alpha},\ \ln\left(\frac{C_{n,0} - C_n}{C_{n,0}}\right) = \ln(k_{id}) + \alpha \ln(t) \tag{10}$$

$$\ln q_n = \ln\beta + K_s \ln t \tag{11}$$

where, C_n(mg-N/L) is the nitrate concentration at time t (min), $k_{r1}(min^{-1})$ is the pseudo-first-order reaction rate constant, k_m is the reaction rate constant with the estimated reaction order n, q_n (mg-N/g-$ZVI_{1.5}$) is the adsorbed nitrate amount at time t, $q_{n,e}$ (mg-N/g-$ZVI_{1.5}$) is the equilibrium adsorption t of nitrate, k_{a1} (min^{-1}) is the pseudo-first-order adsorption rate constant, k_{a2}(g-$ZVI_{1.5}$/mg-N·min) is the pseudo-second-order adsorption rate constant, k_{id} (min^{-1}) is the constant for the intra-particle diffusion model, while α is the constant for the adsorption mechanism. K_S is the constant of double constant model and β is a constant.

3. Results and discussion

3.1. Changes in solution composition during denitrification

The reaction process as defined by changes in the solution composition are shown in Fig. 2. Over time, the concentration of NO_3^- progressively decreased while that of both NH_3-N and Fe^{2+} concurrently increased with the reaction proceeding essentially to completion in the first 15 min, where the NO_3^- concentration decreased from 25 mg/L to 2.2 mg/L. Thereafter, the reaction rate declined and was similar with little denitrification occurring in the interval from 60 min to 120 min. The final concentration of NO_3^- was 1.5 mg/L after 120 min, with cumulative removal rate of 93.9%. Correspondingly, the concentration of NH_3 increased antithetically to that of NO_3^- over time with a maxima of 23.5 mg/L after 120 min. A similar total nitrogen (TN) concentration (25.0 mg/L initial) to that after 120 min (24.8 mg/L) suggested that the NO_3^- was efficiently denitrified to NH_3 in the experiment with an absence of alternative reactions such as denitrification of NO_3^- to N_2, which would have invoked a net loss of TN from the system. Of considerable interest, however, was the presence of a short-lived NO_2^- reactive intermediate most prominent during the period of the highest rate of denitrification in the initial 10 min of the batch experiment (Fig. 2a, b).

Solute concentrations of Fe^{2+} and Fe^{3+} also increased over time. Dissolved Fe^{2+} increased in a similar pattern to both pH and NH_3 (Fig. 2) signifying the progressive dissolution of the $ZVI_{1.5}$ in the acidic solute. The final concentration of Fe^{2+} was 487 mg/L, while pH

Fig. 2. Concentrations of NO_3^- (a), NO^-_2 (b), NH^+_3 (c), TN (d), Fe^{2+} (e), Fe^{3+} (f) and pH (g) during the denitrification experiment. (25 mg/L NO_3^-, 1 g $ZVI_{1.5}$ Error bars represent one standard deviation (n = 3).

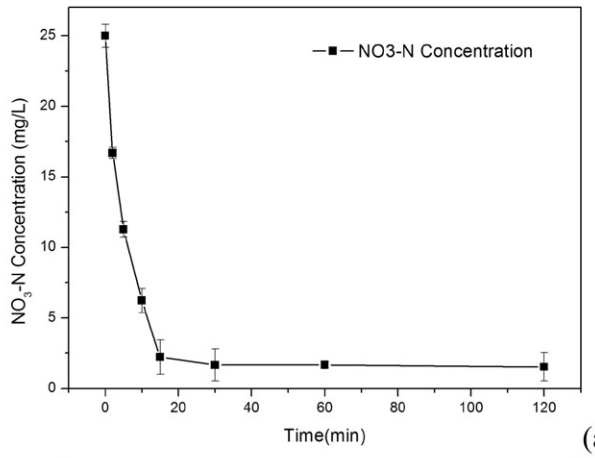
NO3-N Concentration
NO3-N Concentration (mg/L)
Time(min)

(a)

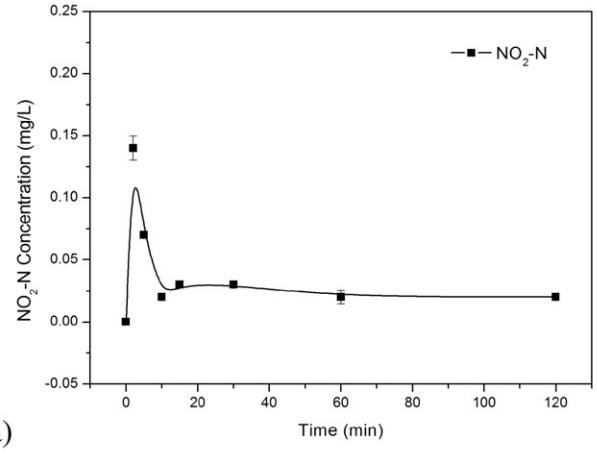
NO2-N
NO2-N Concentration (mg/L)
Time (min)

(b)

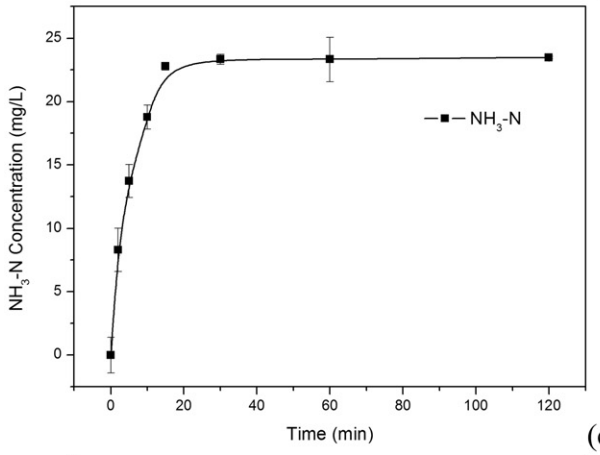
NH3-N
NH3-N Concentration (mg/L)
Time (min)

(c)

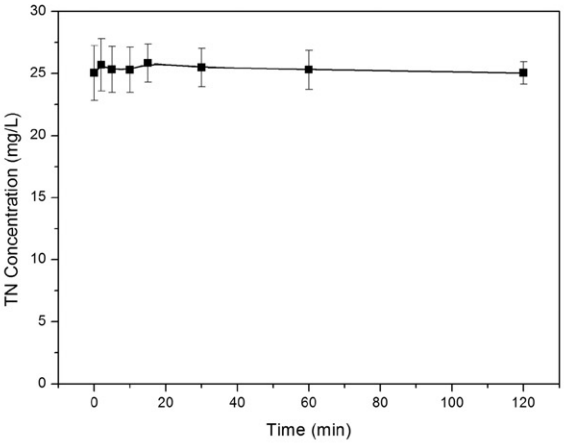
TN Concentration (mg/L)
Time (min)

(d)

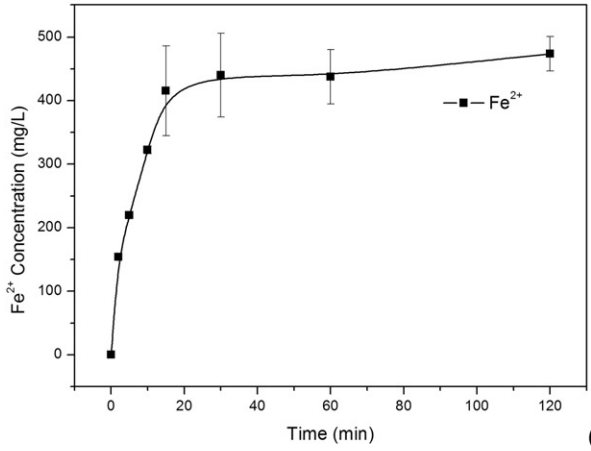
Fe2+
Fe2+ Concentration (mg/L)
Time (min)

(e)

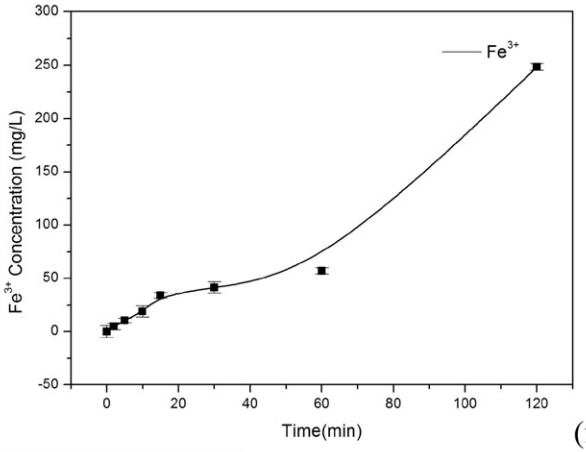
Fe3+
Fe3+ Concentration (mg/L)
Time(min)

(f)

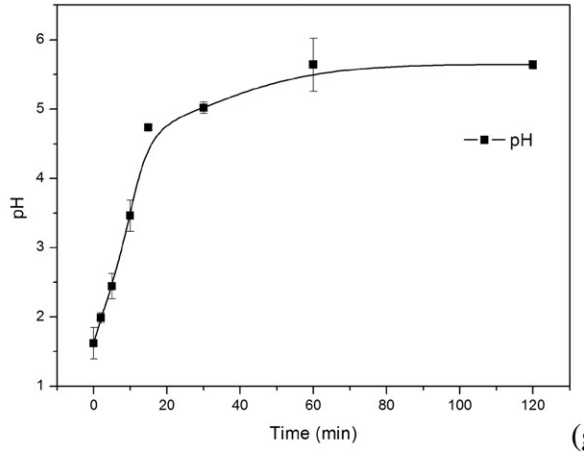
pH
pH
Time (min)

(g)

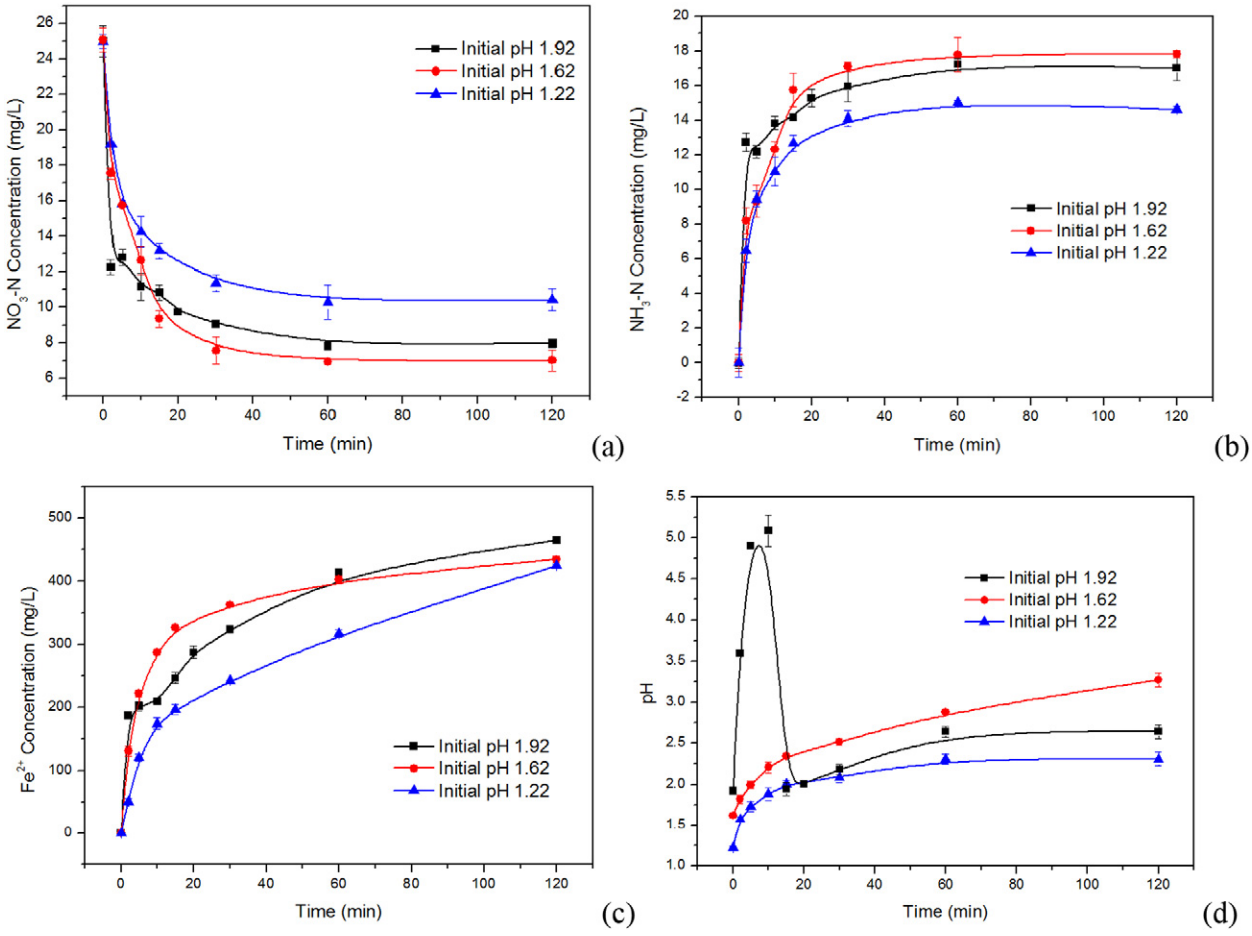

Fig. 3. Impact of pH on NO_3^- (a), NH_3^+ (b), Fe^{2+} (c) concentrations and pH (d) (25 mg/L NO_3^-, 0.416 g/L $ZVI_{1.5}$). Error bars represent one standard deviation (n = 3).

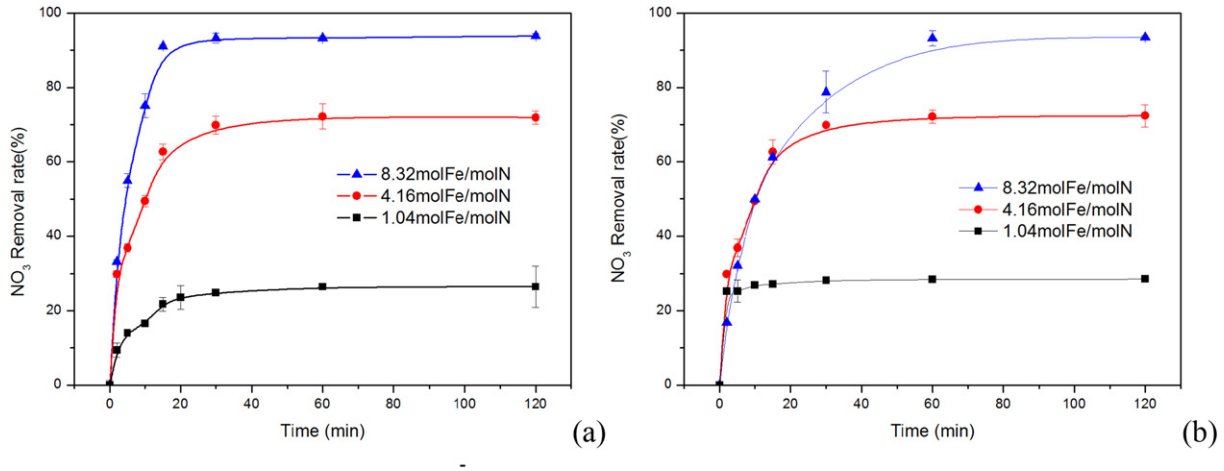

Fig. 4. Impact of the $ZVI_{1.5}$:N molar ratios on NO^-_3 removal, (a), different $ZVI_{1.5}$ dose (25 mg/L NO_3^-, 0.832, 0.416, 0.104 g/L $ZVI_{1.5}$), (b), different initial NO_3^- concentration (12.5, 25, 100 mg/L NO_3^-, 0.416 g/L $ZVI_{1.5}$). Error bars represent one standard deviation (n = 3).

increased to from ca. 1.6 to 5.5 at the end of the 120 min experiment. Dissolved Fe^{3+} also increased during the reaction, initially slowly, with a final concentration of 248 mg/L. The extent of the $ZVI_{1.5}$ dissolution over 120 min based on the final Fe^{2+} concentration was approximately 65% of all dissolved Fe, with Fe^{3+} comprising approximately 35%. Dissolved Fe^{3+} continued to increase in the last 60 mins. In this period, little NO_3^- had been reduced indicating that Fe^{3+} was a by-product of the reaction. It was noted that the solution turned pale yellow under anaerobic conditions consistent with at least partial formation of $Fe(OH)_2$ from the Fe^{2+} suggesting an even higher extent of $ZVI_{1.5}$ dissolutions than indicated by the final Fe^{2+} concentration. Furthermore, upon exposure to the atmosphere the solution became yellow indicating likely oxygen ingress and oxidation of $Fe(OH)_2$ to α-FeOOH (Mukherjee et al., 2016).

Table 1
Kinetic parameters of nitrate removal by $ZVI_{1.5}$ for different $ZVI_{1.5}$:N molar ratios.

Kinetic model	NO_3^- (mg/L-N)	ZVI (g/L)	Parameters		R^2	ZVI:N ratios	NO_3^- (mg/L-N)	ZVI (g/L)	Parameters		R^2
			$k_{r1}(min^{-1})$						$k_{r1}(min^{-1})$		
Pseudo first order reaction	25	0.125	1.70×10^{-3}		0.543	1.04	100	0.5	1.30×10^{-3}		0.179
	25	0.5	8.50×10^{-3}		0.535	4.16	25	0.5	8.50×10^{-3}		0.535
	25	1	1.96×10^{-2}		0.499	8.32	12.5	0.5	2.57×10^{-2}		0.639
			k_{rn}	n					k_{rn}	n	
nth	25	0.125	2.00×10^{-31}	22.49	0.951	1.04	100	0.5	4.50×10^{-32}	16.62	0.84
order reaction	25	0.5	1.02×10^{-5}	4.19	0.970	4.16	25	0.5	1.02×10^{-5}	4.19	0.970
	25	1	3.80×10^{-2}	1.54	0.990	8.32	12.5	0.5	7.61×10^{-1}	2.53	0.990
			$k_{a1}(min^{-1})$	q_e(mgN/gZVI)					$k_{a1}(min^{-1})$	q_e(mgN/gZVI)	
Pseudo first order adsorption	25	0.125	0.080	38.503	0.909	1.04	100	0.5	0.062	11.855	0.915
	25	0.5	0.073	23.774	0.962	4.16	25	0.5	0.073	23.774	0.962
	25	1	0.034	18.793	0.852	8.32	12.5	0.5	0.092	24.946	0.959
			k_{a2} (gZVI/mgN·min)	q_e(mgN/gZVI)					k_{a2} (gZVI/mgN·min)	q_e(mgN/gZVI)	
Pseudo second order adsorption	25	0.125	3.541×10^{-3}	66.225	0.999	1.04	100	0.5	2.474×10^{-2}	68.966	1.000
	25	0.5	6.077×10^{-3}	45.045	0.999	4.16	25	0.5	6.077×10^{-3}	45.045	0.999
	25	1	1.382×10^{-2}	28.902	0.999	8.32	12.5	0.5	3.308×10^{-3}	30.769	0.998
			$k_{id}(min^{-1})$	α					$k_{id}(min^{-1})$	α	
Intra-particle diffusion	25	0.125	5.4669	19.61	0.716	1.04	100	0.5	0.8754	60.706	0.755
	25	0.5	3.6183	13.665	0.707	4.16	25	0.5	3.6359	13.618	0.711
	25	1	2.3036	10.018	0.623	8.32	12.5	0.5	2.711	4.1442	0.860
			K_s	β					K_s	β	
double constants	25	0.125	0.264	3.092	0.874	1.04	100	0.5	0.0354	4.075	0.906
	25	0.5	0.234	2.811	0.876	4.16	25	0.5	0.235	2.809	0.878
	25	1	0.242	2.397	0.759	8.32	12.5	0.5	0.424	1.574	0.909

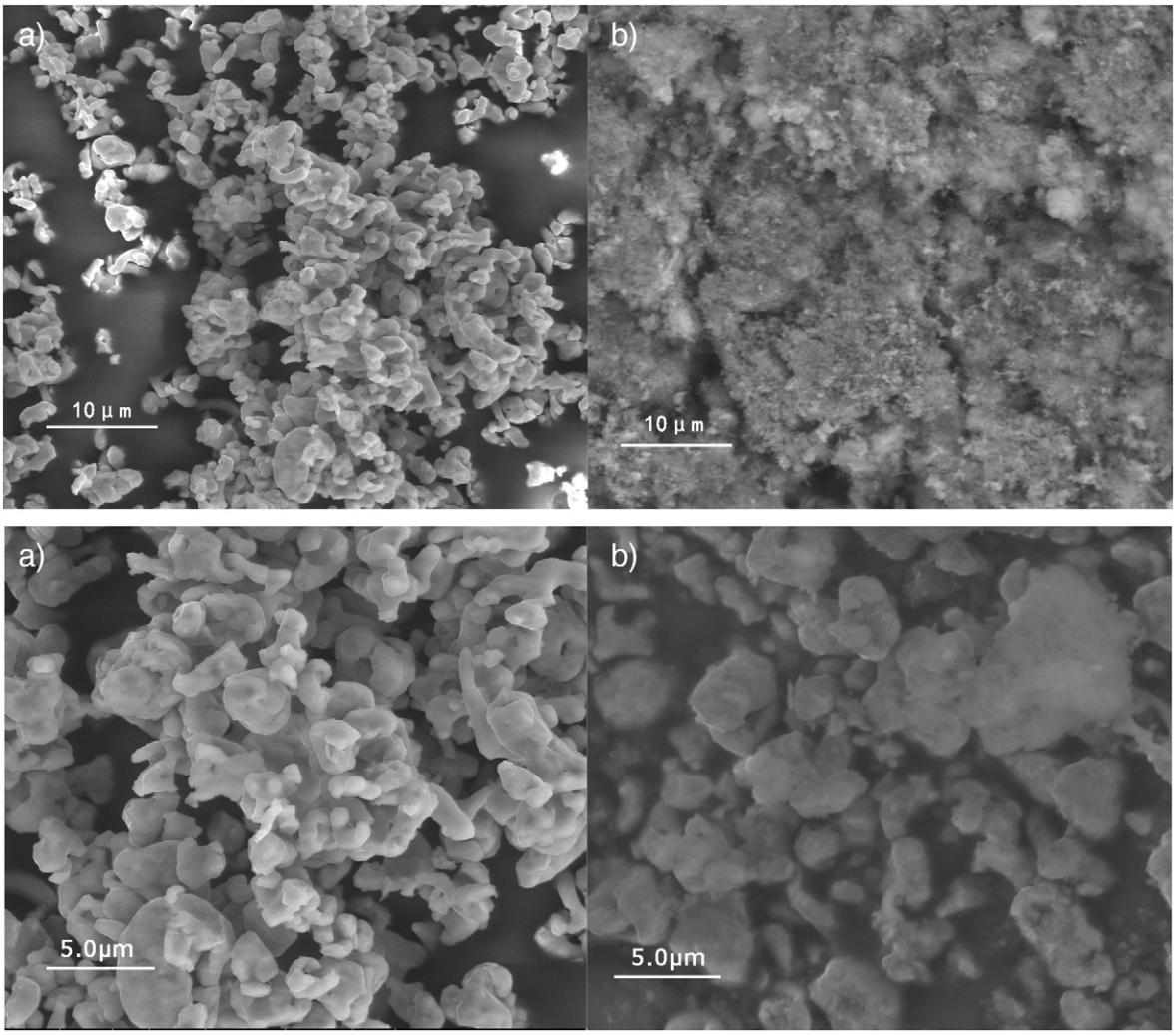

Fig. 5. Scanning Electron Microscopy (SEM) images of $ZVI_{1.5}$ before (a) and after (b) reaction.

3.2. Effect of initial pH on the denitrification rate and extent

It is evident that the initial reaction pH may substantially influence both the rate and extent of denitrification (Zawaideh and Zhang, 1998). The most common concept is that the lower pH the better for ZVI-based denitrification (Huang et al., 1998; Li et al., 2007). In this study, we focused on the influence of pH below 2 on denitrification. Interestingly, however, the lowest initial experimental pH of 1.22 (60 mmol H^+/L) was the least efficient for denitrification with both the lowest maximum rates and also the least extent of conversion of NO_3^- to NH_3 of approximately 60% (Fig. 3a). Hence, there may be a lower pH threshold for efficient denitrification. In contrast, at both pH 1.62 and 1.92 (24 and 12 mmol H^+/L respectively) a similar extent of denitrification of approximately 68 and 72%, respectively was achieved (Fig. 3a). Some distinct differences were apparent, however, between the efficiency of denitrification, particularly in the initial 20 min of the reaction. While more Fe^{2+} was generated at pH 1.62 (24 mmol H^+/L, Fig. 3c), less NO_3^- was denitrified and less NH_3 produced (Fig. 3a, b). Most notable, however, was the substantial, transient increase in solute pH for the highest initial pH (1.92) case (Fig. 3d) to approximately 5.1 after 15 min of reaction, as a result of OH^- production via the anaerobic corrosion of Fe^0. It appeared that although the initial rate of denitrification and NH_3 production was greatest at the highest initial pH of 1.92, with lowest hydrogen ion concentration of 12 mmol/L, there was a deficit in hydrogen ions to meet the immediate requirements during the period of the highest rate of denitrification. This hydrogen ion deficit led to the observed transient increase in pH, and a concomitant reduction in denitrification efficiency. In light of this behavior, and to assess whether NO_3^- reduction could be reinitiated, an additional 12 mmol of HCl was added to the solution after 15 min reaction time. Thereafter, the total acidity was the same as that of the pH 1.62 experiment (24 mmol H^+/L) while the adjusted pH after 20 min was the same as in the pH 1.22 (60 mmol H^+/L) experiment. At the end of the 120 min experiment, the rate of denitrification and NH_3 production were slightly less than that of the pH 1.62 experiment, likely in part due to the low initial acidity, the subsequent pH adjustment, and resultant perturbations to the experimental conditions.

3.3. Effect of $ZVI_{1.5}$:N molar ratios on the denitrification rate and extent

Experiments were conducted to study the effects of the stoichiometric ratio of $ZVI_{1.5}$ to NO_3^- (as N) at a range of Fe:N molar ratios (1.04, 4.16 and 8.33). It is evident that both the rate and extent of denitrification were substantially enhanced by increasing the Fe:N molar ratios from 1.04 to 8.33 (Fig. 4). After 120 min residual NO_3^- concentrations were 18.4, 7.0, and 1.69 mg/L, for the 1.04, 4.16 and 8.33 Fe:N molar ratios, equating to 26%, 72% and 95% removal, respectively. In an alternative approach to varying the $ZVI_{1.5}$:N molar ratios by adjusting $ZVI_{1.5}$ concentrations, NO_3^- concentrations were also varied between 12.5 and 100 mg/L to yield the same set of $ZVI_{1.5}$:N molar ratios of 1.04, 4.16 and 8.33. After 120 min residual NO_3^- concentrations were 70.0, 7.0, and 0.65 mg/L, for the 1.04, 4.16 and 8.33 Fe:N molar ratios, equating to 29%, 72% and 94% removal, respectively. This phenomenon also was observed by other researchers, (Wei et al., 2016; Liang et al., 2014) where a higher Fe:N ratio could materially improve the rate of denitrification.

3.4. Kinetics of nitrate reduction for different $ZVI_{1.5}$:N molar ratios

The changes in the NO_3^- concentration as described by the pseudo-first-order reaction model, pseudo-first-order adsorption, the pseudo-second-order adsorption, the double constant equation, and the intra-particle diffusion model are illustrated in Table 1. The modelling results suggest that the pseudo-first-order reaction kinetic model is unsuitable for all conditions, since these models are not relevant under ZVI- or nZVI-limiting conditions (Kim et al., 2016; Yang and Lee, 2005), although the estimated pseudo-first-order rate constant correlates well with the ZVI dose. For an nth order reaction, the reaction rate constant increases and the reaction order decreases as the ZVI dose is increased, also as the initial NO_3^- concentration decreased. This is consistent with the findings of other studies (Kim et al., 2016; Yang and Lee, 2005). For the adsorption-based kinetic equations, the pseudo-second-order adsorption equation provides the best fit, especially showing a similar q_e to $ZVI_{1.5}$:N molar ratios, suggesting that the $ZVI_{1.5}$:N molar ratios influence the adsorption capacity. Furthermore, the NO_3^- adsorption capacity of $ZVI_{1.5}$, which was estimated on the basis of pseudo-first-order adsorption or pseudo-second-order adsorption, was lower than nZVI (Kim et al., 2016), but higher than the corresponding capacity of other adsorbents such as activated carbon or activated sepiolite (Öztürk and Bektaş, 2004). This result confirms the utility of $ZVI_{1.5}$ as a NO_3^- adsorbent. Alternatively, the double constant model fits well and the intra-particle diffusion model is a poor fit to the data, implying that intra-particle diffusion does not limit the rate of NO_3^- sorption on $ZVI_{1.5}$. However, the mass transfer across the external boundary layer of a solid or the boundary-layer diffusion of nitrate is a dominant factor in NO_3^- adsorption by ZVI, as mentioned above and is reflected by the good fit of the experimental results to the pseudo-second-order adsorption rate equation.

3.5. Morphological and mineralogical characterisation of $ZVI_{1.5}$ pre- and post-denitrification reaction

Scanning Electron Microscopy (SEM) images of $ZVI_{1.5}$ before and after reaction are shown in Fig. 5a, b. Most notable is the smooth surface and mostly separate $ZVI_{1.5}$ particles prior to the denitrification reaction. Following the denitrification reaction, however, the $ZVI_{1.5}$ particles had an irregular surface and formed larger aggregates reflecting both partial dissolution and loss of Fe^{2+} to solution but also possible adhesion of reactive surfaces by reaction by-products.

X-ray diffraction patterns of fresh and reacted $ZVI_{1.5}$ are shown in Fig. 6. For fresh $ZVI_{1.5}$, the three characteristic peaks occurred at 44.7°, 65.0° and 82.3° 2θ consistent with 110, 200, and 211 faces of crystalline α-Fe (JCPDS No. 06-0696). These three peaks were still conserved after the denitrification experiments indicating the presence of unreacted Fe^0. However, additional peaks occur at 35.4°, 36.1°, 57.1° and 62.7°2θ consistent with the presence of goethite (α-FeOOH), a reaction product also noted elsewhere (Li et al., 2015a, 2015b; Sun et al., 2006; Zhang, 2003).

X-ray photoelectron spectroscopy (XPS) was also used to investigate the surface composition and chemical state of $ZVI_{1.5}$ pre- and post- the denitrification reaction (Fig. 7a–e, Tables 3 and 4). The fresh $ZVI_{1.5}$

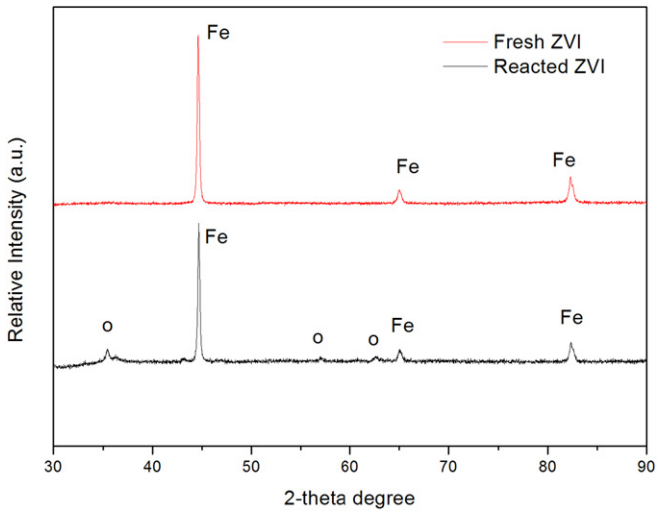

Fig. 6. Mineralogy of $ZVI_{1.5}$ before and after reaction.

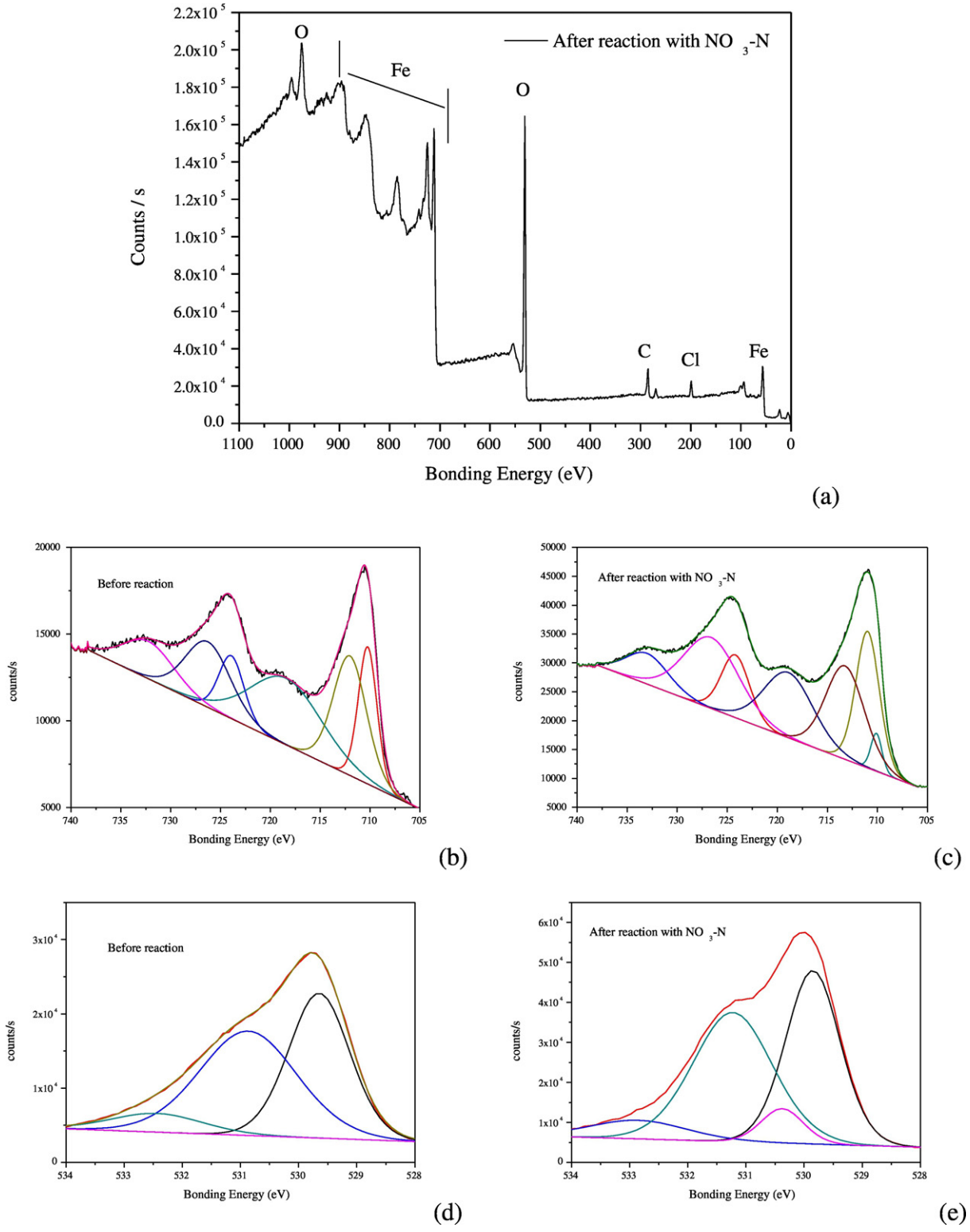

Fig. 7. X-ray photoelectron spectroscopy spectra before and after reaction, total element analysis, (a), Fe_{2p} analysis before (b) and after reaction (c), and O_{1s} analysis of before (d) and after reaction (e).

Table 2
Relative concentrations of a range of elements in fresh and reacted $ZVI_{1.5}$ determined by X-ray photoelectron spectroscopy (XPS).

ZVI	Fe(%)	Cl(%)	C(%)	O (%)	O/C
Fresh	14.43	–	26.27	59.30	2.257
Reacted	25.31	3.69	16.76	54.23	3.236

consisted principally of Fe, O and C. It is likely that the C was present due to contamination during sample preparation (Henderson and Demond, 2007). Following the denitrification experiment, Cl was present reflecting the addition of HCl to adjust the initial reaction pH.

Detailed analysis of XPS Fe_{2p} spectra in the region 705–740 eV, and the peak position of $Fe_{2p3/2}$ indicated that an oxide surface, principally

Table 3
The peak position of $Fe_{2p3/2}$ and physical structure determined by X-ray photoelectron spectroscopy (XPS).

ZVI	Peak A (eV)	Structure	Peak B (eV)	Structure	Peak C (eV)	Structure
Fresh (ratio)	710.251 (14.4%)	FeO	–	–	712.033 (22.4%)	Fe_2O_3
Reacted (ratio)	710.099 (2.4%)	FeO	710.975 (18.4%)	FeOOH	713.237 (20.8%)	Fe_2O_3

Table 4
The peak position of O_{1s} and physical structure determined by X-ray photoelectron spectroscopy (XPS).

ZVI	Peak A (eV)	Structure	Peak B (eV)	Structure	Peak C (eV)	Structure	Peak D (eV)	Structure
Fresh (ratio)	529.646 (42.7%)	O^{2-} (Fe_2O_3)	530.866 (49.0%)	O^{2-} (FeO)	–	–	532.442 (8.3%)	H_2O
Reacted (ratio)	529.843 (41.1%)	O^{2-} (Fe_2O_3)	530.315 (6.4%)	O^{2-} (FeO)	531.293 (44.7%)	OH^-	532.958 (7.8%)	H_2O

of FeO at 710.25 eV and Fe_2O_3 at 712.03 eV was present on the fresh $ZVI_{1.5}$ (Fig. 7b–c, Table 4). The presence of Fe oxides armouring $ZVI_{1.5}$ has also been noted by (Cai et al., 2014; Jiang et al., 2015; Ju et al., 2015). Following the denitrification reaction, a new peak at 710.97 eV corresponding to α-FeOOH was present in agreement with the XRD analysis. (Ismail et al., 1996).

Detailed analysis of the XPS O_{1s} spectra in the region 528–534 eV in the fresh and reacted $ZVI_{1.5}$ can be deconvoluted into a number of overlapping peaks corresponding to O^{2-}, OH^- and adsorbed H_2O. Similar to the results of the XPS Fe_{2p} spectra, the XPS O_{1s} spectra also indicated major changes in the surface composition of the fresh and reacted $ZVI_{1.5}$. In particular, FeO substantially decreased (49.0% to 6.4%), Fe_2O_3 concentrations were similar (42.7% to 41.1%) while substantial α-FeOOH (44.7%) was formed presumably due to the hydrous oxidation of FeO (Fig. 7 (d–e)). The formation of the various oxides and hydroxyl oxides gives some insight into the changes that may occur at the surface of reacted ZVI, for instance in a permeable reactive barrier, subject to varying redox conditions (Jeong et al., 2012; Cheng et al., 2014).

3.6. Proposed mechanism and reaction pathways

A combined solute and solids analysis of the denitrification of NO_3^- by $ZVI_{1.5}$ has allowed detailed insights to be drawn regarding solute-solid interaction. Based on the solution data analysis and detailed mineralogical and surface analysis of the $ZVI_{1.5}$, possible reaction pathways for NO_3^- denitrification of $ZVI_{1.5}$ were proposed (Fig. 8).

An important outcome of the solution analysis was the identification of the presence of a short-lived NO_2^- reactive intermediate that was only apparent during the highest rate of denitrification (Fig. 2a, b). The presence of NO_2^-, only measureable in the initial stages of the reaction, highlights its importance during the stepwise denitrification of NO_3^- to NH_3 as outlined in Fig. 8 and reactions (9) and (10) below:

$$Fe^0_{(s)} + NO^-_{3(aq)} + 2H^+_{(aq)} \rightarrow Fe^{2+}_{(aq)} + NO^-_{2\ (aq)} + H_2O_{(l)} \quad (12)$$

$$3Fe^0_{(s)} + NO^-_{2(aq)} + 8H^+_{(aq)} \rightarrow 3Fe^{2+}_{(aq)} + NH^+_{4\ (aq)} + 2H_2O_{(l)} \quad (13)$$

yielding an overall stoichiometric reaction:

$$4Fe^0_{(s)} + NO^-_{3(aq)} + 10H^+_{(aq)} \rightarrow 4Fe^{2+}_{(aq)} + NH^+_{4\ (aq)} + 3H_2O_{(l)} \quad (14)$$

Analysis of the $ZVI_{1.5}$ pre- and post-denitrification indicate that while a pre-existing armour of FeO and Fe_2O_3 is present on its surface, two reactions are likely to occur. The first is the dissolution of these oxides under the prevailing acidic conditions of the denitrification experiment while the second is the dissolution of continually exposed Fe^0 at the surface to liberate Fe^{2+} into solution. Contemporaneously, there is a surface-mediated denitrification reaction occurring at the surface of

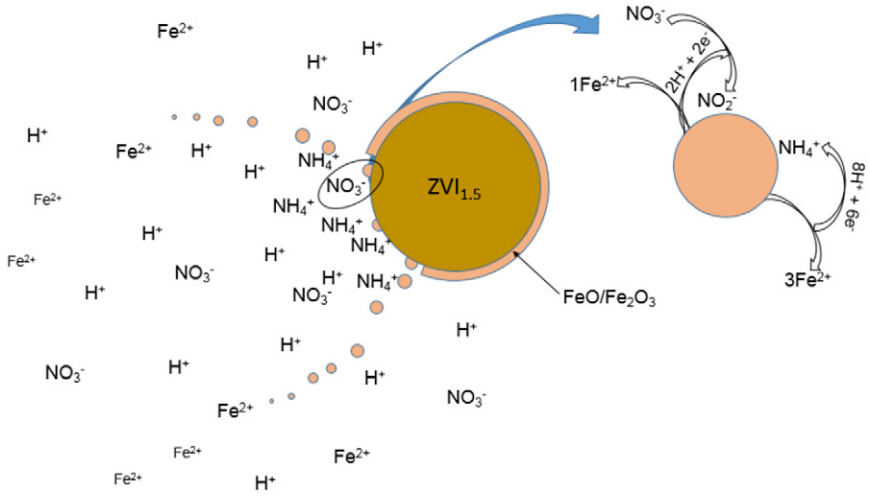

Fig. 8. Proposed mechanism and reaction pathways.

the $ZVI_{1.5}$ with a reactive NO_2^- intermediate prominent in the reduction of NO_3^- to NH_4^+ (reactions 12 to 14). This reaction pathway has also been demonstrated elsewhere (Kim et al., 2016; Yang and Lee, 2005). In contrast, the development of reaction products such as goethite (α-FeOOH) on the $ZVI_{1.5}$ may also play a part in reducing the rate of denitrification via surface passivation as the reaction proceeds, particularly where progressive hydrogen ion consumption allows a substantial increase in solute pH.

4. Conclusions

Several aspects regarding the chemical reduction of NO_3^- by $ZVI_{1.5}$ particles have been investigated in this work. Based on our findings, the following conclusions can be drawn:

(1). Under the experimental conditions used here, denitrification is rapid with the conversion of NO_3^- to NH_3 essentially complete within 120 min with substantial Fe^{2+} released into solution. An initial pH of 1.62 was the most suitable for denitrification.
(2). Nitrite forms an important reaction intermediate during denitrification to NH_3 with substantial Fe^{2+} released into solutions as a result of $ZVI_{1.5}$ oxidation and dissolution.
(3). Both pseudo-first-order and pseudo-second-order adsorption kinetic equations provided a good fit for the observed NO_3^- removal. Increasing the concentration of $ZVI_{1.5}$ resulted in an increase in reaction rate and denitrification efficiency. The same of $ZVI_{1.5}$: NO_3^- ratio with different initial $ZVI_{1.5}$ or NO_3^- concentrations had similar reaction rates and denitrification efficiency.
(4). Mineralogical analysis of the $ZVI_{1.5}$ by XRD indicated the formation of α-FeOOH (goethite) after denitrification. Surface analysis by XPS indicated the presence of Fe_2O_3 and FeO on the surface of the fresh $ZVI_{1.5}$, with the majority of the latter converted to goethite following the denitrification process.

Acknowledgements

The authors are grateful to the reviewers for their comments which significantly improved the quality of the manuscript.

References

Alidokht, L., Khataee, A.R., Reyhanitabar, A., 2011. Reductive removal of Cr(VI) by starch-stabilized Fe^0 nanoparticles in aqueous solution. Desalination 1-3 (270), 105–110.
An, Y., Dong, Q., Zhang, K., 2014. Bioinhibitory effect of hydrogenotrophic bacteria on nitrate reduction by nanoscale zero-valent iron. Chemosphere 103, 86–91.
Audi-Miro, C., Cretnik, S., Torrento, C., 2015. C, Cl and H compound-specific isotope analysis to assess natural versus Fe(0) barrier-induced degradation of chlorinated ethenes at a contaminated site. J. Hazard. Mater. 299, 747–754.
Belghit, H., Colas, C., Bristeau, S., 2015. Liquid chromatography-high-resolution mass spectrometry for identifying aqueous chlordecone hydrate dechlorinated transformation products formed by reaction with zero-valent iron. Int. J. Environ. Anal. Chem. 2 (95), 93–105.
Cai, X., Gao, Y., Sun, Q., 2014. Removal of co-contaminants Cu (II) and nitrate from aqueous solution using kaolin-Fe/Ni nanoparticles. Chem. Eng. J. 244, 19–26.
Cheng, K.Y., Kaksonen, A.H., Douglas, G.B., 2014. Sequential in situ hydrotalcite precipitation and biological denitrification for the treatment of high-nitrate industrial effluent. Bioresour. Technol. 172, 373–381.
Cho, D., Song, H., Schwartz, F.W., 2015. The role of magnetite nanoparticles in the reduction of nitrate in groundwater by zero-valent iron. Chemosphere 125, 41–49.
Choe, S., Liljestrand, H.M., Khim, J., 2004. Nitrate reduction by zero-valent iron under different pH regimes. Appl. Geochem. 3 (19), 335–342.
Deliyanni, E., Peleka, E., Lazaridis, N., 2007. Comparative study of phosphates removal from aqueous solutions by nanocrystalline akaganéite and hybrid surfactant-akaganéite. Sep. Purif. Technol. 3 (52), 478–486.
Devlin, J.F., Eedy, R., Butler, B.J., 2000. The effects of electron donor and granular iron on nitrate transformation rates in sediments from a municipal water supply aquifer. J. Contam. Hydrol. 1–2 (46), 81–97.
Dong, J., Zhao, Y., Zhao, R., 2010. Effects of pH and particle size on kinetics of nitrobenzene reduction by zero-valent iron. J. Environ. Sci. (China) 11 (22), 1741–1747.
Fagan, R., McCormack, D.E., Dionysiou, D.D., 2016. A review of solar and visible light active TiO2 photocatalysis for treating bacteria, cyanotoxins and contaminants of emerging concern. Mater. Sci. Semiconductor Processing. SI1 42, 2–14.
Fateminia, F.S., Falamaki, C., 2013. Zero valent nano-sized iron/clinoptilolite modified with zero valent copper for reductive nitrate removal. Process. Saf. Environ. Prot. 4 (91), 304–310.
Fewtrell, L., 2004. Drinking-water nitrate, methemoglobinemia, and global burden of disease: a discussion. Environ. Health Perspect. 14 (112), 1371–1374.
Guo, X., Yang, Z., Liu, H., 2015. Common oxidants activate the reactivity of zero-valent iron (ZVI) and hence remarkably enhance nitrate reduction from water. Sep. Purif. Technol. 146, 227–234.
Guo, X., Yang, Z., Dong, H., 2016. Simple combination of oxidants with zero-valent-iron (ZVI) achieved very rapid and highly efficient removal of heavy metals from water. Water Res. 88, 671–680.
Han, W., Fu, F., Cheng, Z., 2016. Studies on the optimum conditions using acid-washed zero-valent iron/aluminum mixtures in permeable reactive barriers for the removal of different heavy metal ions from wastewater. J. Hazard. Mater. 302, 437–446.
Henderson, A.D., Demond, A.H., 2007. Long-term performance of zero-valent iron permeable reactive barriers: a critical review. Environ. Eng. Sci. 4 (24), 401–423.
Hosseini, S.M., Kholghi, M., Vagharfard, H., 2012. Numerical and meta-modeling of nitrate transport reduced by nano-Fe/Cu particles in packed sand column. Transp. Porous Media 1 (94), 149–174.
Huang, C., Wang, U., Chiu, P., 1998. Nitrate reduction by metallic iron. Wat. Res. 2258–2265, 32–38.
Huang, G., Huang, Y., Hu, H., 2015. Remediation of nitrate–nitrogen contaminated groundwater using a pilot-scale two-layer heterotrophic–autotrophic denitrification permeable reactive barrier with spongy iron/pine bark. Chemosphere 130, 8–16.
Hwang, Y., Kim, D., Shin, H., 2011. Mechanism study of nitrate reduction by nano zero valent iron. J. Hazard. Mater. 2-3 (185), 1513–1521.
Ismail, H.M., Cadenhead, D.A., Zaki, M.I., 1996. Surface reactivity of iron oxide pigmentary powders toward atmospheric components: XPS and gravimetry of oxygen and water vapor adsorption. J. Colloid Interface Sci. 2 (183), 320–328.
Jeong, J., Kim, H., Kim, J., 2012. Electrochemical removal of nitrate using ZVI packed bed bipolar electrolytic cell. Chemosphere 2 (89), 172–178.
Jiang, C., Xu, X., Megharaj, M., 2015. Inhibition or promotion of biodegradation of nitrate by *Paracoccus* sp. In the presence of nanoscale zero-valent iron. Sci. Total Environ. 530-531, 241–246.
Ju, Y., Liu, X., Li, Z., 2015. Environmental application of millimetre-scale sponge iron (S-Fe^0) particles (i): pretreatment of cationic triphenylmethane dyes. J. Hazard. Mater. 283, 469–479.
Jun, D., Yuanyuan, L., Xueqing, Z., 2013. Fedeg/zndeg PRB technology for the remediation of PCBs contaminated groundwater. Appl. Mech. Mater. 295-298, 1364–1367.
Jung, S., Lee, M., Kim, J., 2011. Speed-dependent emission of air pollutants from gasoline-powered passenger cars. Environ. Technol. 11 (32), 1173–1181.
Kapoor, A., Viraraghavan, T., 1997. Nitrate removal from drinking water - review. J. Environ. Eng. 4 (123), 371–380.
Kay, D., Bartram, J., Pruss, A., 2004. Derivation of numerical values for the world health organization guidelines for recreational waters. Water Res. 5 (38), 1296–1304.
Kim, D., Hwang, Y., Shin, H., 2016. Kinetics of nitrate adsorption and reduction by nanoscale zero valent iron (NZVI): effect of ionic strength and initial pH. J. Civ. Eng. 1 (20), 175–187.
Li, C., Chen, Y., Yen, W., 2007. Pressurized CO_2/zero valent iron system for nitrate removal. Chemosphere 2 (68), 310–316.
Li, J., Qin, H., Guan, X., 2015a. Premagnetization for enhancing the reactivity of multiple zerovalent iron samples toward various contaminants. Environ. Sci. Technol. 24 (49), 14401–14408.
Li, X., Wang, H., Hu, C., 2015b. Characteristics of biofilms and iron corrosion scales with ground and surface waters in drinking water distribution systems. Corros. Sci. 90, 331–339.
Liang, L., Sun, W., Guan, X., 2014. Weak magnetic field significantly enhances selenite removal kinetics by zero valent iron. Water Res. 49, 371–380.
Lin, Y., Weng, C., Chen, F., 2008. Effective removal of AB24 dye by nano/micro-size zero-valent iron. Sep. Purif. Technol. 1 (64), 26–30.
Ling, L., Pan, B., Zhang, W., 2015. Removal of selenium from water with nanoscale zero-valent iron: mechanisms of intraparticle reduction of Se(IV). Water Res. 71, 274–281.
Liu, H., Qian, T., Zhao, D., 2013. Reductive immobilization of perrhenate in soil and groundwater using starch-stabilized ZVI nanoparticles. Chin. Sci. Bull. 2 (58), 275–281.
Liu, Y., Li, S., Chen, Z., 2014. Influence of zero-valent iron nanoparticles on nitrate removal by *Paracoccus* sp. Chemosphere 108, 426–432.
Long, Y., Zhang, C., Du, Y., 2014. Enhanced reductive dechlorination of polychlorinated biphenyl-contaminated soil by in-vessel anaerobic composting with zero-valent iron. Environ. Sci. Pollut. Res. 6 (21), 4783–4792.
Luo, J., Song, G., Liu, J., 2014. Mechanism of enhanced nitrate reduction via micro-electrolysis at the powdered zero-valent iron/activated carbon interface. J. Colloid Interface Sci. 435, 21–25.
Ma, Z., Yang, Y., Jiang, Y., 2015. Effects of anions on bio-chemical degradation of nitrate in groundwater. Environ. Earth Sci. 5 (74), 3985–3992.
Mukherjee, R., Kumar, R., Sinha, A., 2016. A review on synthesis, characterization, and applications of nano zero valent iron (NZVI) for environmental remediation. Crit. Rev. Environ. Sci. Technol. 5, 443–466.
Olson, M.R., Blotevogel, J., Borch, T., 2014. Long-term potential of in situ chemical reduction for treatment of polychlorinated biphenyls in soils. Chemosphere 114, 144–149.
Öztürk, N., Bektaş, T.E., 2004. Nitrate removal from aqueous solution by adsorption onto various materials. J. Hazard. Mater. 1-2 (112), 155–162.
Peng, L., Liu, Y., Gao, S., 2015. Evaluation on the nanoscale zero valent iron based microbial denitrification for nitrate removal from groundwater. Sci. Report. 5, 12331.

Penon, O., Marin, M.J., Amabilino, D.B., 2016. Iron oxide nanoparticles functionalized with novel hydrophobic and hydrophilic porphyrins as potential agents for photodynamic therapy. J. Colloid Interface Sci. 462, 154–165.
Ren, L., Ni, S., Liu, C., 2015. Effect of zero-valent iron on the start-up performance of anaerobic ammonium oxidation (anammox) process. Environ. Sci. Pollut. Res. 4 (22), 2925–2934.
Schwindaman, J.P., Castle, J.W., Rodgers, J.H., 2014. Biogeochemical process-based design and performance of a pilot-scale constructed wetland for arsenic removal from simulated Bangladesh groundwater. Water Air Soil Pollut. 6 (225), 1–11.
Shin, K., Cha, D.K., 2008. Microbial reduction of nitrate in the presence of nanoscale zero-valent iron. Chemosphere 2 (72), 257–262.
Siciliano, A., 2015. Use of nanoscale zero-valent iron (NZVI) particles for chemical denitrification under different operating conditions. Metals 3 (5), 1507–1519.
Simeonidis, K., Mourdikoudis, S., Kaprara, E., 2016. Inorganic engineered nanoparticles in drinking water treatment: a critical review. Environ. Sci.: Water Res. Technol. 1 (2), 43–70.
Sismanoglu, T., Karakus, S., Birer, O., 2015. Preparation and characterization of antibacterial *Senegalia* (Acacia) Senegal/iron-silica bio-nanocomposites. Appl. Surf. Sci. B 354, 250–255.
Soleymanzadeh, M., Arshadi, M., Salvacion, J.W.L., 2015. A new and effective nanobiocomposite for sequestration of Cd(ii) ions: nanoscale zerovalent iron supported on sineguelas seed waste. Chem. Eng. Res. Des. 93, 696–709.
Su, Y., Adeleye, A.S., Huang, Y., 2014a. Simultaneous removal of cadmium and nitrate in aqueous media by nanoscale zerovalent iron (NZVI) and au doped NZVI particles. Water Res. 63, 102–111.
Su, Y., Adeleye, A.S., Zhou, X., 2014b. Effects of nitrate on the treatment of lead contaminated groundwater by nanoscale zerovalent iron. J. Hazard. Mater. 280, 504–513.
Sun, Y., Li, X., Cao, J., 2006. Characterization of zero-valent iron nanoparticles. Adv. Colloid Interf. Sci. 1-3 (120), 47–56.
Waclawek, S., Nosek, J., Cadrova, L., 2015. Use of various zero valent irons for degradation of chlorinated ethenes and ethanes. Ecol. Chem. Eng. S. 4 (22), 577–587.
Wang, T., Lin, J., Chen, Z., 2014. Green synthesized iron nanoparticles by green tea and eucalyptus leaves extracts used for removal of nitrate in aqueous solution. J. Clean. Prod. 83, 413–419.
Wei, X., Gao, N., Li, C., 2016. Zero-valent iron (ZVI) activation of persulfate (PS) for oxidation of bentazon in water. Chem. Eng. J. 285, 660–670.
Xu, J., Pu, Y., Qi, W., 2017. Chemical removal of nitrate from water by aluminum-iron alloys. Chemosphere 166, 197–202.
Yang, G.C.C., Lee, H., 2005. Chemical reduction of nitrate by nanosized iron: kinetics and pathways. Water Res. 5 (39), 884–894.
Yoshino, H., Kawase, Y., 2013. Kinetic modeling and simulation of zero-valent iron wastewater treatment process: simultaneous reduction of nitrate, hydrogen peroxide, and phosphate in semiconductor acidic wastewater. Ind. Eng. Chem. Res. 50 (52), 17829–17840.
Zawaideh, L.L., Zhang, T.C., 1998. The effects of pH and addition of an organic buffer (HEPES) on nitrate transformation in Fe-0-water systems. Water Sci. Technol. 7 (38), 107–115.
Zhang, W., 2003. Nanoscale iron particles for environmental remediation: an overview. J. Nanopart. Res. 5, 323–332.
Zhang, Y., Li, Y., Li, J., 2011. Enhanced removal of nitrate by a novel composite: nanoscale zero valent iron supported on pillared clay. Chem. Eng. J. 2 (171), 526–531.
Zhang, M., Lu, J., Xu, Z., 2015. Removing polybrominated diphenyl ethers in pure water using Fe/Pd bimetallic nanoparticles. Front. Environ. Sci. Eng. 5SI (9), 832–839.
Zhang, M., Xu, Z., Teng, Y., 2016. Non-target effects of repeated chlorothalonil application on soil nitrogen cycling: the key functional gene study. Sci. Total Environ. 543, 636–643.
Zhao, L., Dong, H., Kukkadapu, R.K., 2015. Biological redox cycling of iron in nontronite and its potential application in nitrate removal. Environ. Sci. Technol. 9 (49), 5493–5501.
Zhou, D., Li, Y., Zhang, Y., 2014a. Column test-based optimization of the permeable reactive barrier (PRB) technique for remediating groundwater contaminated by landfill leachates. J. Contam. Hydrol. 168, 1–16.
Zhou, Y., Yang, J., Wang, X., 2014b. Bio-beads with immobilized anaerobic bacteria, zero-valent iron, and active carbon for the removal of trichloroethane from groundwater. Environ. Sci. Pollut. Res. 19 (21), 11500–11509.
Zhou, X., Lv, B., Zhou, Z., 2015. Evaluation of highly active nanoscale zero-valent iron coupled with ultrasound for chromium (VI) removal. Chem. Eng. J. 281, 155–163.